Retrieval of source parameters of an event of the 2000 West Bohemia earthquake swarm assuming an anisotropic crust

Dirk Rößler[1)], Frank Krüger[2)], Ivan Pšenčík[3)], Georg Rümpker[4)]

1) University of Potsdam, K.-Liebknecht-Str. 24, 14476 Golm, FR Germany, E-mail: diroess@rz.uni-potsdam.de
2) University of Potsdam, K.-Liebknecht-Str. 24, 14476 Golm, FR Germany, E-mail: kruegerf@geo.uni-potsdam.de
3) Geophysical Institute AS CR, Boční II/1401, 141 31 Prague 4, Czech Republic, E-mail: ivan@ig.cas.cz
4) University of Frankfurt/Main, Feldbergstr. 47, 60323 Frankfurt/Main, FR Germany, E-mail: rumpker@geophysik.uni-frankfurt.de

Summary

We propose an inversion scheme to retrieve characteristics of seismic point sources, which in contrast to common practice, takes into account anisotropy. If anisotropy is neglected durig inversion, the moment tensors retrieved from seismic waves due to sources situated in anisotropic media may be biased. Instead of the moment tensor, the geometry of the source is retrieved directly in our inversion; if necessary, the moment tensor can be then determined from the source geometry. The source geometry is defined by the orientation of the slip vector and the fault normal as well as the strength of the event given by the size of the slip and the area of the fault. This approach allows direct interpretation of the source geometry in terms of shear and tensile faulting. It also makes possible to identify volumetric source changes that occur during rupturing.

We apply the described algorithm to one event of the year 2000 earthquake swarm episode in West Bohemia (Central Europe). For inversion we use information of the direct P waves. The structure is approximated by three different models determined from travel-time observations. The models are inhomogeneous isotropic, inhomogeneous anisotropic, and homogeneous anisotropic. For these models we obtain seismic moments $M_T = 3.2 - 3.8 * 10^{14}$ Nm and left-lateral near-vertical oblique normal faulting on a N-S trending rupture surface. The rupture surface is consistent with fault-plane solutions of earlier studies and with the spatial distribution of other events during this swarm. The event seems to be accompanied by a small amount of crack opening. The amount of crack opening is slightly reduced when the inhomogeneous anisotropic model is assumed, but it persists. This result seems to indicate a role of fluids on the triggering of this event.

Keywords: seismic source, tensile earthquake, anisotropy, West Bohemia

1 Introduction

Seismic moment tensors are retrieved from waveforms to describe the orientation and the strength of point sources. They are routinely determined under the assumption that the medium

[0]Seismic Waves in Complex 3-D Structures, Report 16 (Department of Geophysics, Charles University, Prague 2006), pp. 283-306

around the source and along the ray-path is isotropic. Anisotropic material properties are usually neglected during the inversion. However, the radiation pattern of seismic sources may be affected by anisotropy (see e.g. *Kawasaki* and *Tanimoto*, 1981; *Gajewski*, 1993; *Pšenčík* and *Teles*, 1996; *Rößler et al.*, 2004). This may lead to the occurrence of apparent non-double-couple moment-tensor components (see e.g. *Rößler et al.*, 2004; *Vavryčuk*, 2005; *Rößler et al.*, 2006). On the contrary, true volumetric components may become invisible in moment tensors. The effect of anisotropy on moment tensors depends on the strength of anisotropy and on the orientation of the anisotropic elastic tensor with respect to the geometry of the source.

Moment tensors can be decomposed into the double-couple component (DC) quantifying the amount of shear faulting, the compensated-linear-vector-dipole component (CLVD), and the isotropic component (ISO) providing information on possible volumetric source changes that occur during faulting (*Jost* and *Herrmann*, 1989; *Aki* and *Richards*, 2002). Faulting events that comprise volumetric source changes are also called tensile earthquakes.

In practice, non-double-couple components are frequently observed and interpreted in terms of tensile faulting (see e.g. *Sykes*, 1967; *Solomon* and *Julian*, 1974; *Julian et al.*, 1997; *Horálek et al.*, 2000; *Dahm et al.*, 2000; *Vavryčuk*, 2002; *Foulger et al.*, 2004; *Vavryčuk*, 2001). Observed volumetric components may be indicative of the role of fluids during rupturing and mineral phase changes at greater depth or may image existing pathways enabling fluid migration in carbonhydrate production fields. In these cases accurate and indisputable determination of tensile components is of primary interest. Without knowledge of anisotropy at the source, the reliability of interpretations of the moment tensor in terms of volumetric source changes must be questioned (*Vavryčuk*, 2005; *Rößler et al.*, 2006). We therefore propose an inversion scheme for point sources in inhomogeneous anisotropic media. For such sources, we directly invert observed seismograms for the direction of slip and the fault normal.

We apply the inversion algorithm to one event that occurred during earthquake swarm in West Bohemia in 2000.

2 Seismograms due to elementary sources in anisotropic structures

For seismic waves travelling in anisotropic media the i-th component u_i of the far-field complex-valued displacement at a location $\mathbf{x}$ due to a moment point source at $\mathbf{x}_0$ is given in the ray-theoretical high-frequency approximation (*Pšenčík* and *Teles*, 1996):

$$u_i(\mathbf{x},t) = g_i(\mathbf{x}) \left[\frac{\rho(\mathbf{x}_0)c(\mathbf{x}_0)}{\rho(\mathbf{x})c(\mathbf{x})}\right]^{1/2} \frac{Df^{(A)}(t-\tau(\mathbf{x}))}{|\Omega_M(\mathbf{x})|^{1/2}} \exp\left[i\frac{\pi}{2}k_s - i\frac{\pi}{2}k(\mathbf{x}_0,\mathbf{x})\right]. \tag{1}$$

Actual seismograms are given by the real part of the displacement $\mathrm{Re}(u_i(\mathbf{x},t))$. Note that the appoximation (1) is limited to P waves and well separated S waves. The formula (1) suffers from the limitations of the ray theory, see *Červený* (2001). We should expect its lower accuracy in in caustic regions of both waves and in singular directions of P waves. The quantity D in (1) denotes the directivity given by

$$D(\mathbf{x}_0,\theta,\phi) = \frac{g_j(\mathbf{x}_0)M_{jk}\,p_k(\mathbf{x}_0)}{4\pi\rho(\mathbf{x}_0)c(\mathbf{x}_0)}. \tag{2}$$

The directivity (2) represents a spreading-free amplitude at the source. It should not be confused with the directional dependence of amplitudes due to source finiteness. It depends on the moment tensor M_{jk}, the polarisation and the slowness vectors g_j and p_k, respectively, as well as the phase velocity c and the density ρ at the source. The slowness vector p_k at the source is specified by the angles θ and ϕ.

In (1), Ω_M is related to the relative geometrical spreading $|\Omega_M|$, $g_i(\mathbf{x})$ is the polarisation vector at $\mathbf{x}$, and $f^{(A)}$ is the analytical signal corresponding to the source time function. The integer quantities k and k_s are the indices of the trajectory and of the source, respectively (see *Pšenčík* and *Teles*, 1996, for a detailed description). Note that we are referring to a right-handed coordinate system: N,E,Z$\rightarrow x_1, x_2, x_3$ but observed seismograms are recorded in the coordinate system: N,E,Z with Z pointing positive up.

For dislocation point sources, the source geometry is described by the unit slip vector s_p, the unit normal n_q to the fault plane, and the product of the size of the slip s and the fault area A_0. Elastic moduli c_{jkpq}, that describe medium properties in the vicinity of the source, and source geometry define the moment tensor M_{jk} (*Aki* and *Richards*, 2002):

$$M_{jk} = c_{jkpq} s_p n_q s A_0. \tag{3}$$

From (3), we can see that different properties of the moment tensor arise from sources in isotropic and anisotropic media. For example, shear faulting in anisotropic media may produce moment tensors which correspond to tensile earthquakes in isotropic media, i.e. shear faulting accompanied by some amount of opening or closing of the fault during rupturing (see e.g. *Rößler et al.*, 2004; *Vavryčuk*, 2005).

We can also express the moment tensor in (3) in terms of the source tensor D_{pq}:

$$M_{jk} = c_{jkpq} D_{pq}, \tag{4}$$

where D_{pq} is formed by the dyadic product of the slip and the fault normal

$$D_{pq} = \frac{1}{2} s A_0 \begin{pmatrix} 2s_1n_1 & s_1n_2 + s_2n_1 & s_1n_3 + s_3n_1 \\ s_1n_2 + s_2n_1 & 2s_2n_2 & s_2n_3 + s_3n_2 \\ s_1n_3 + s_3n_1 & s_2n_3 + s_3n_2 & 2s_3n_3 \end{pmatrix}. \tag{5}$$

Elements of the source tensor D_{pq} make up 6 elementary sources σ_i, which are components of the vector $\boldsymbol{\sigma}$

$$\boldsymbol{\sigma}^T = sA_0(s_1n_1, s_1n_2 + s_2n_1, s_1n_3 + s_3n_1, s_2n_2, s_2n_3 + s_3n_2, s_3n_3). \tag{6}$$

Inserting (2), (3), and (6) into (1), we can express the seismograms in terms of the elementary sources σ_l

$$\mathrm{Re}\left(u_i(\mathbf{x}, t)\right) = \mathrm{Y}_{il}\mathrm{Re}\left(f^{(A)}(t - \tau(\mathbf{x}))\exp\left[i\frac{\pi}{2}k_s - i\frac{\pi}{2}k(\mathbf{x}_0, \mathbf{x})\right]\right)\sigma_l. \tag{7}$$

For Y_{il} see Appendix A.

3 Inverse problem

The left-hand side of (7) is determined from observed seismograms. All terms forming Y_{il} are obtained numerically for inhomogeneous anisotropic media using the software package ANRAY (*Pšenčík*, 1998). The system of equations (7) corresponding to observations at different receivers is then solved for the 6 elementary sources σ_l. Hereby, we use a linear least square approach to minimise the squared misfit $\boldsymbol{\epsilon}^T\boldsymbol{\epsilon}$, where $\boldsymbol{\epsilon}^T$ is the misfit of both sides of Eq. (7) (see *Menke*, 1989). The residual R is formed by normalisation of the squared misfit

$$R = \frac{\boldsymbol{\epsilon}^T\boldsymbol{\epsilon}}{\mathrm{Re}\,(u_i)\,\mathrm{Re}\,(u_i)}. \tag{8}$$

In this way, the misfit is related to the observed amplitudes and residuals for events with different strength are comparable.

We seek the source vector $\vec{\sigma}$ by inversion of seismograms of observed direct P waves. The inversion is carried out in the time domain. Misalignment of observed data and synthetic seismograms often occurs due to inaccurate phase picking. For time-domain inversion this may cause spurious non-shear components in retrieved source geometries. Phase alignment is therefore carried out in 3 steps prior to inversion:

1. Observed phases are manually picked. A time window for inversion is defined.
2. Within the time window observed phases are manually aligned with the computed synthetic seismograms.
3. Automatic cross-correlation is applied. A threshold based on the correlation coefficient may be used to define if data are to be included in inversion.

The efficiency of the algorithm is demonstrated by inversion of seismograms generated by synthetic sources in *Rößler et al.* (2005).

A singular value decomposition of D_{pq} in (5) yields the eigenvalues $\nu_1 = sA_0/2\,(s_i n_i + 1)$, $\nu_2 = 0$, $\nu_3 = sA_0/2\,(s_i n_i - 1)$ (compare *Vavryčuk*, 2005). The corresponding (normalised) eigenvectors are $\mathbf{e}_1 = (\mathbf{s}+\mathbf{n})/\,|\mathbf{s}+\mathbf{n}|$, $\mathbf{e}_2 = (\mathbf{s}\times\mathbf{n})/\,|\mathbf{s}\times\mathbf{n}|$, and $\mathbf{e}_3 = (\mathbf{s}-\mathbf{n})/\,|\mathbf{s}-\mathbf{n}|$, where $\times$ denotes the vectorial cross product. In the following we calculate the slip inclination δ, i.e. the angle between the direction of the slip and the fault normal, $\cos(\delta) = |s_i n_i|$, from the retrieved σ_l forming D_{pq}

$$cos(\delta) = \frac{\nu_1 + \nu_3}{\nu_1 - \nu_3}. \tag{9}$$

For pure shear faulting, $\delta = 90°$, but $\delta \gtrless 90°$ for tensile earthquakes (volumetric source changes, see Appendix B). However, for sources other than dislocation point sources, e.g. explosions or faultings on non-planar fault surfaces, inversions using (7) will yield $\nu_2 \neq 0$. Occurrence of $\nu_2 \neq 0$ may be an indication of an inadequate description of the seismic source by (3) or insufficient modelling of ray-path effects by Y_{il}. From a combination of the eigenvalues and the eigenvectors of D_{pq} we get s_i, n_i, and $A_0 s$ (see Appendix B). In fact, we obtain two vectors but we cannot uniquely identify from observations of seismograms which is s_i and which is n_i. We get two conjugate fault planes that are perpendicular to s_i or n_i. These two planes are associated with the rupture plane and the auxiliary plane. They can form any angle. For shear faulting both planes are perpendicular. As in other source inversions, the rupture plane must be identified from additional information such as aftershock distribution or known fault-zone geometry. The area of the fault A_0 and the length of the slip s cannot be separated. From inversion we can only get their product $A_0 s$.

Given the retrieved source geometry, the moment tensor, which is usually sought in seismological practice, may be immediately computed from (3). We decompose the moment tensor into its double-couple (DC) and non-double-couple components, i.e. the compensated-linear-vector-dipole (CLVD) and the isotropic component (ISO). Several different decompositions of M_{ij} have been proposed (see e.g. *Silver* and *Jordan*, 1982; *Jost* and *Herrmann*, 1989; *Vavryčuk*, 2002). Herein, we use equations of *Vavryčuk* (2002) that relate the moment-tensor components to the complete moment tensor. The (real or apparent) non-double-couple components have often been interpreted in terms of volumetric source changes connected to the faulting process. In anisotropic media, this interpretation might not be correct because the (apparent) non-double-couple moment-tensor components may be a consequence of neglected anisotropy (*Rößler et al.*, 2004; *Vavryčuk*, 2005; *Rößler et al.*, 2006). If, however, anisotropy is taken into account and the slip inclination δ differs from 90°, this is a more reliable indication of real volumetric source changes. The slip inclination is therefore considered as an important parameter during inversion. Possible conclusions made from the slip inclination and from the standard non-double-couple components may be later compared.

As a measure of strength of the event, we calculate the seismic moment M_T from the moment tensor (*Silver* and *Jordan*, 1982):

$$\mathrm{M}_T = \sqrt{\Sigma_{ij} M_{ij}^2/2}. \tag{10}$$

4 Source retrieval for a M_L=3.1 earthquake from West Bohemia

Studies of source mechanisms for West Bohemia swarm episode in 1997 revealed evidence for tensile faulting, i.e. shear faulting that is accompanied by volumetric source changes during faulting. Such volume changes were found from interpretation of the non-double-couple components of retrieved moment tensors (*Vavryčuk*, 2002). However, seismic anisotropy observed in this region (*Vavryčuk*, 1993; *Růžek et al.*, 2003; *Málek et al.*, 2005) was neither accounted for during interpretations nor during inversions for moment tensors.

We apply our inversion algorithm to one earthquake that occurred during the year 2000 earthquake swarm episode in Vogtland/West Bohemia. This earthquake swarm represents the most recent period of intense seismic activity in the region. It started on August 28, 2000 and lasted for 4 months. The events occurred on a fault, oriented in N-S direction at depths between 8 and 11 km. Accurate hypocentre locations are provided by *Boušková* (2005). The swarm has been subdivided into nine separate phases. The selected event forms the onset of the fifth phase. Hypocentre parameters are 50.2085° N, 12.4576° E, 9.243 km depth, source time is October 15, 2000, 16:36:48 (*Fischer, pers. comm.*). Till now, a detailed study of source mechanisms of the year 2000 earthquake swarm has not yet been performed but indications of fluid related earthquake triggering have been found, e.g. by *Fischer* and *Horálek* (2005); *Hainzl* and *Ogata* (2005) and *Parotidis et al.* (2005). Observations by *Hainzl* and *Ogata* (2005) indicate that changes in pore pressure by high-pressure crustal fluids may be important for the triggering of events at the beginning and also during the fifth phase of the swarm.

In addition to the permanent stations in the region, temporary stations were installed by the University of Potsdam, the WEBNET group, the Central Seismological Observatory and the GeoForschungsZentrum Potsdam at different periods during the swarm (see Tab. 1, Fig. 1, and *Klinge et al.*, 2003). The selected event occurred at a time of maximum station coverage. Note that although many stations were available, ray coverage was non-uniform. For example, only one station in SE direction can be used.

Several homogeneous and inhomogeneous isotropic velocity models were published for the focal area in West Bohemia (see e.g. *Novotný*, 1996; *Málek et al.*, 2004). Three anisotropic/isotropic models used in this study and referred to as models I-III, see Fig. 2, Tables 2-4, were derived by *Málek et al.* (2005) and *Vavryčuk* (1993).

Model I is a vertically inhomogeneous isotropic model derived by *Málek et al.* (2005), see Fig. 2 and Table 2.

Model II is a vertically inhomogeneous, weak anisotropy model also derived by *Málek et al.* (2005), see Fig. 2 and Table 3. The model has been derived from P waves only.

Model III is homogeneous and transversely isotropic. See Fig. 2 for averaged isotropic velocities and Tab. 4 for the elastic moduli. It has been derived from S-wave splitting and S-P travel time differences using effective medium theory (*Vavryčuk*, 1993).

We invert three-component displacement seismograms of the P waves recorded at 18 stations, for which the amplitude transfer functions are accurately known (see Fig. 1 for their locations and Tab. 1 for their coordinates). Stations with unknown amplitude characteristics are not included. Seismograms are uniformly resampled to 0.01 s sampling interval. A time window of 0.4 s around the P wavelet is used for inversion. The similarity between the shape of observed and modelled waveforms is expressed by the cross-correlation coefficient. The cross-correlation coefficient for most traces is above 0.9. We exclude seismograms with complicated P wavelets that have cross-correlation coefficients below 0.6. Observed P waves are generally characterised by high signal-to-noise ratios and clear onsets (Fig. 3). The corner frequency of the studied event is around 10 Hz (Fig. 4). To guarantee that the inversion is independent of the source-time function of the event, we low-pass filter data and synthetic seismograms at 10 Hz.

Using the models I-III similar fault-plane solutions are obtained (see Fig. 5 and Tab. 5) and the residuals are similarly reduced. Wavelets match well at all stations except the station LBC (Fig. 6, trace 9). The plane oriented in N-S direction is identified as the rupture plane. It can be associated with the map of the fault zone obtained from located earthquake foci (*Fischer*, 2003). The event is therefore characterised by left-lateral oblique normal faulting on a N-S oriented fault plane dipping steeply towards the West. This orientation is similar to results obtained by *Fischer* and *Horálek* (2005) using the FOCMEC algorithm (*Snoke*, 2003). The retrieved dip-slip component is increased for model III as compared to the models I and II. The seismic moment varies in the range $3.2 - 3.8 * 10^{14}$ Nm. Using an empirical relation for local magnitudes M_L in West Bohemia (*Hainzl* and *Fischer*, 2002) we find M_L=3.1.

Retrieved sources comprise a small amount of tensile component (crack opening) indicated by $\delta < 90°$ for all three models (see Tab. 5). The deviation from pure shear faulting (tensile character) is smallest for the inhomogeneous anisotropic model II. Here, the slip vector deviates off the fault plane by 3.2° (Tab. 5). A small increase in the tensile character is observed for the inhomogeneous isotropic model I. The non-double-couple components of the resulting moment tensors are also small and nearly equal for models I and II (Tab. 5). The largest tensile components and largest non-double-couple moment-tensor components are retrieved for the homogeneous anisotropic model III. For all velocity models I-III, the eigenvalues of retrieved D_{pq} in (5) are $\nu_1 \gg \nu_2$ and $\nu_3 \gg \nu_2$. This indicates that the determined source mechanisms are in accordance with the model for dislocation point sources assumed in (3)-(5) and (9). The differences in solution resulting from models I/II and III can be explained by the structural differences causing differently modulated amplitudes in the modelled wavefield and different ray take-off angles at the source (Fig. 7). Take-off directions are indistuingishable for rays in the models I and II. Therefore, the small differences in source geometry for models I and II most probably result from anisotropy.

In our data example it seems that the retrieved source mechanism is more similar to a shear source when assuming more structural complexity including vertical inhomogeneity and P-wave anisotropy. Adding information on anisotropy from observations of S waves to the inhomogeneous anisotropic model II could intensify this effect. However, accounting for structural inhomogeneity takes the largest effects on retrieved source parameters. Similar observations were made by *Ramos-Martínez* and *McMechan* (2001) using a finite-difference approach.

Only the inhomogeneous anisotropic model II contains information on structural complexity and anisotropy. This model is therefore used to test the sensitivity of the inversion to variations of the station distribution and of the weight given to the data of a station. First we perform jackknife tests, i.e. we randomly omit 10% or 25% of all traces available from all stations. The procedure is repeated 200 times (see Fig. 8 for results of jackknife tests). We find that fault orientation, slip inclination, and components of moment tensors are well constrained if the number of traces is randomly reduced by 10% (Fig. 8a). For most realisations the slip inclination varies between 85° and 89°. The retrieved double-couple and isotropic components are in the range of 75-90% and 0-10%, respectively. When reducing the number of traces by 25% (Fig. 8b), fault planes show a wider range of variability. Slip inclinations are in the same range as for the 10%-jackknife test. The distribution of double-couple and isotropic components is broadened and a greater number with small DC occur. For most realisations, isotropic components are positive. We can therefore rule out that the observed tensile source component is an artefact of the station distribution.

Next we carry out bootstrap tests, i.e. we modify the weight of one single station during inversion by feeding the data of this station 1, 2, 5, 10, 20, 50 or 100 times into the system of equations (7), see Fig. 9. The procedure is repeated for every station while the weights of the remaining stations are kept equal. For a station with high weight factor the inversion aims to fit the amplitudes of this station preferentially. If rays to one station are of special importance for the inversion, e.g. for isolated station location, the solution can be stabilised by increasing the weight for this station. However, inversions may become unstable if amplitudes are inappropriately modelled at the station that is weighted higher. This can be the case for unknown near-station structure.

Retrieved fault-plane solutions show only minor variability for all bootstrap tests (Fig. 9a). Except for station LBC the variations of the slip inclination, the moment-tensor components, and the residuals are close to each other (see Fig. 9b). The mean values of the slip inclinations are slightly larger than values for unchanged initial conditions (see Tab. 5). However, small standard deviations indicate that the tensile components are significant. Increasing weight for station LBC causes deviation of all quantities. Observed DC<70% in Fig. 9 is caused by overweighting station LBC. The influence of LBC cannot be explained by the station location because it is situated in a direction of dense ray coverage (compare Fig. 1). Therefore, it must be caused by the mismodelling of the P-wave amplitude (Fig. 6). Omitting LBC during inversion leads to increase in shear character ($\delta = 88°$ for otherwise unchanged initial conditions and model II) and to an increase in the double-couple component of the moment tensor as well as a slight rotation of the fault orientation (see Tab. 5). However, a small amount of non-shear component remains. A similar trend is also found for the models I and III (see Tab. 5). Therefore, the observed tensile component does not seem to be an artefact of mismodelled structure along a ray to a particular station.

The principle directions of the local stress field (P and T axes) are stable during testing (see Figs. 8, 9). They indicate compression in SE–NW direction and extension in SW–NE wich is similar to the stress field observed before in West Bohemia and Central Europe (*Wirth et al.*, 2000; *Hinzen*, 2003; *Plenefisch* and *Klinge*, 2003)

We have also carried out computations to evaluate the influence of mismodelled source depth. For the calculations of synthetic seismograms we considered all three velocity models and put sources between 6 km and 14 km depth with a step of 500 m. Note that the depth uncertainty due to the localisation algorithm is about 100 m (*Fischer, pers. comm.*). Additional errors in source locations may occur due to ignored anisotropy in the localisation algorithm (*Málek et al.*, 2005).

Residuals as well as retrieved slip inclinations and seismic moment tensors show sensitivity to source depth in all three models I-III (Figs. 10-12). The fault orientation is rotated towards a larger strike slip component for shallower event depths.

Assuming the inhomogeneous isotropic model I a minimum residual is reached at 2 km above the localisation depth (Fig. 10). Here, the slip inclination δ indicates almost pure shear faulting. A maximum of the DC moment-tensor component is reached for a source depth below 8 km. The seismic moment and the size of the isotropic moment-tensor component increase whereas the slip inclination decreases monotonously with the assumed source depth.

Similar observations are made for the inhomogeneous anisotropic model II. In contrast to model I, the smallest residuals are observed for source depths between 8 and 9 km, thus closer to the localisation depth, which is 9.24 km. Retrieved seismic moments are slightly increased. In contrast to model I, therefore as an effect of anisotropy, the minimum of the residual function and the CLVD coincide with the maximum of the DC.

For the homogeneous anisotropic model III, the residual function shows a broader minimum at 11-12.3 km source depth, thus significantly below the localised source depth. Seismic moments are slightly larger than for the models I and II. No extremum is observed for the deviatoric moment-tensor components in the considered depth range. The fault plane solutions contain an increased dip-slip component. The different behaviour of the residual function and the source orientation as compared to the models I and II can be partly explained by increased angles of incident waves at the surface. Models I and II contain a near-surface low-velocity zone that is missing in model III. Therefore, angles of incident waves are steeper in models I and II than in model III. Consequently, for sources in model III greater hypocentre depths are required to obtain the same incidence angles at the surface. This explains why the smallest residuals in model III can be found at greater depth than in models I and II. As a result, different take-off angles in models I/II and III lead to a rotation of the retrieved source mechanisms.

5 Discussion and conclusions

We have introduced an algorithm to retrieve the geometry of point sources in anisotropic media. Decoupling the source geometry from the elastic properties of the medium surrounding the source allows direct interpretation of the retrieved source mechanism in terms of possible volumetric source changes. For interpretation we assume dislocation point sources characterised by the normal to the fault plane, the direction of the slip, the fault area, and the size of the slip. Fault normal and slip vector may be arbitrarily oriented. Thus, we allow shear faulting as well as tensile faulting. Deviations from the dislocation model may be found by an eigenvalue analysis of the source tensor D_{pq}. The inversion scheme is based on fitting of synthetic seismograms to observed ones. For computation of synthetic seismograms we apply ray methods for isotropic or anisotropic media, which represent a basis of the ANRAY software package (*Pšenčík*, 1998). The algorithm is therefore time-effective and applicable in standard data processing. The success of the proposed inversion scheme depends on the accuracy of the used structural model.

The inversion algorithm was applied to one earthquake of the earthquake swarm that occurred in West Bohemia in the year 2000. We observe $M_T \approx 3.4 * 10^{14}$ Nm and left-lateral strike oblique normal faulting. The source mechanism retrieved for this event is in agreement with the model for dislocation point sources. A small amount of crack opening is indicated. Although it is only slight, this feature seems to be generally stable and significant for different structural models, different assumptions about source depth and for changing station coverage. The local stress field obtained from the retrieved source mechanisms is in agreement with other observations in West Bohemia and Central Europe. The results of inversion are constrained by jackknife and bootstrap tests. Accounting for structural 1D inhomogeneity has a significant effect on the solution. Taking into account anisotropy in the inhomogeneous model II leads to a slight decrease in the tensile component of the obtained source mechanism. In model II anisotropy is derived from information of P waves only. Changes in anisotropy caused by considering S waves are expected to further influence the results. Effects due to more complicated source-time functions are diminished by excluding frequencies above the corner frequency of the event. The influence of intrinsic attenuation, near-source inhomogeneity, e.g., crack induced changes in near-source anisotropy, and source finiteness are not considered here.

Future applications of the introduced inversion algorithm can be seen where accurate determination of source mechanisms is of superior interest and where well-defined anisotropic velocity models exist, e.g. in borehole vicinity or in carbonhydrate production fields.

Acknowledgements

Support of the German Science Foundation (DFG, grants KR1935/1-1 and KR1935/1-3), of the Charles University, Prague through the MAGMA project, of the Geophysical Institute, Acad. Sci. of the CR, and of the consortium project SW3D is appreciated. We thank the following people for data provision: T. Fischer (Geophysical Institute, Acad. Sci. of the CR), Th. Plenefisch (SZGRF), S. Funke (University of Leipzig), J. Wassermann (University of Munich) as well as colleagues and students from the University of Potsdam.

A Equations for source retrieval

Equations (7) can be derived from Eqs. (1), (2), (3), and (6) in the following way:

$$\begin{aligned} u_i(\mathbf{x},t) &= g_i(\mathbf{x}) \left[\frac{\rho(\mathbf{x}_0)c(\mathbf{x}_0)}{\rho(\mathbf{x})c(\mathbf{x})}\right]^{1/2} \frac{Df^{(A)}(t-\tau(\mathbf{x}))}{|\Omega_M(\mathbf{x})|^{1/2}} \exp\left[i\frac{\pi}{2}k_s - i\frac{\pi}{2}k(\mathbf{x}_0,\mathbf{x})\right] \\ &= A_i B_{jk} s_p n_q c_{pqjk} s A_0 f^{(A)}(t-\tau(\mathbf{x})) \exp\left[i\frac{\pi}{2}k_s - i\frac{\pi}{2}k(\mathbf{x}_0,\mathbf{x})\right]. \end{aligned} \tag{A.1}$$

From (A.1), we obtain Eq. (7)

$$\mathrm{Re}\,(u_i(\mathbf{x},t)) = Y_{il}\mathrm{Re}\left(f^{(A)}(t-\tau(\mathbf{x}))\exp\left[i\frac{\pi}{2}k_s - i\frac{\pi}{2}k(\mathbf{x}_0,\mathbf{x})\right]\right)\sigma_l.$$

In (A.1) we use the following notations:

$$A_i = \frac{g_i(\mathbf{x})}{(\rho(\mathbf{x})c(\mathbf{x}))^{1/2}} \frac{1}{|\Omega_M(\mathbf{x})|}, \tag{A.2}$$

$$B_{jk} = \frac{g_j(\mathbf{x}_0)p_k(\mathbf{x}_0)}{4\pi\,(\rho(\mathbf{x}_0)c(\mathbf{x}_0))^{1/2}}, \tag{A.3}$$

$$\begin{aligned}
Y_{i1} &= X_{i1}c_{1111} + X_{i2}c_{1112} + X_{i3}c_{1113} + X_{i4}c_{1122} + X_{i5}c_{1123} + X_{i6}c_{1133},\\
Y_{i2} &= X_{i1}c_{1211} + X_{i2}c_{1212} + X_{i3}c_{1213} + X_{i4}c_{1222} + X_{i5}c_{1223} + X_{i6}c_{1233},\\
Y_{i3} &= X_{i1}c_{1311} + X_{i2}c_{1312} + X_{i3}c_{1313} + X_{i4}c_{1322} + X_{i5}c_{1323} + X_{i6}c_{1333},\\
Y_{i4} &= X_{i1}c_{2211} + X_{i2}c_{2212} + X_{i3}c_{2213} + X_{i4}c_{2222} + X_{i5}c_{2223} + X_{i6}c_{2233},\\
Y_{i5} &= X_{i1}c_{2311} + X_{i2}c_{2312} + X_{i3}c_{2313} + X_{i4}c_{2322} + X_{i5}c_{2323} + X_{i6}c_{2333},\\
Y_{i6} &= X_{i1}c_{3311} + X_{i2}c_{3312} + X_{i3}c_{3313} + X_{i4}c_{3322} + X_{i5}c_{3323} + X_{i6}c_{3333},
\end{aligned} \tag{A.4}$$

where

$$\begin{aligned}
X_{i1} &= A_iB_{11},\\
X_{i2} &= A_i(B_{12} + B_{21}),\\
X_{i3} &= A_i(B_{13} + B_{31}),\\
X_{i4} &= A_iB_{22},\\
X_{i5} &= A_i(B_{23} + B_{32}),\\
X_{i6} &= A_iB_{33}.
\end{aligned} \tag{A.5}$$

B Slip and fault normal from the source tensor

The orientation of the slip s_i, the fault normal n_i, and the product of fault area A_0 and the length of the slip s are determined from the eigenvalues ν_i and the corresponding eigenvectors $\mathbf{e}_i$ of the source tensor D_{ij}. The eigenvalues of D_{ij} are (compare *Vavryčuk*, 2005)

$$\nu_1 = \frac{sA_0}{2}(s_in_i + 1), \quad \nu_2 = 0, \quad \nu_3 = \frac{sA_0}{2}(s_in_i - 1). \tag{B.1}$$

They can be also written as

$$\nu_1 = \frac{sA_0}{4}(\mathbf{s} + \mathbf{n}) \cdot (\mathbf{s} + \mathbf{n}), \quad \nu_2 = 0, \quad \nu_3 = \frac{sA_0}{4}(\mathbf{s} - \mathbf{n}) \cdot (\mathbf{s} - \mathbf{n}). \tag{B.2}$$

The corresponding (normalised) eigenvectors are

$$\mathbf{e}_1 = (\mathbf{s} + \mathbf{n}) / |\mathbf{s} + \mathbf{n}|, \quad \mathbf{e}_2 = (\mathbf{s} \times \mathbf{n}) / |\mathbf{s} \times \mathbf{n}|, \quad \mathbf{e}_3 = (\mathbf{s} - \mathbf{n}) / |\mathbf{s} - \mathbf{n}|, \tag{B.3}$$

where $\times$ denotes the vectorial cross product. Then, s_i, n_i, and A_0s are determined from (B.2) and (B.3)

$$\mathbf{s} = \frac{\mathbf{e}_1\sqrt{\nu_1} + \mathbf{e}_3\sqrt{|\nu_3|}}{\left|\mathbf{e}_1\sqrt{\nu_1} + \mathbf{e}_3\sqrt{|\nu_3|}\right|}, \quad \mathbf{n} = \frac{\mathbf{e}_1\sqrt{\nu_1} - \mathbf{e}_3\sqrt{|\nu_3|}}{\left|\mathbf{e}_1\sqrt{\nu_1} - \mathbf{e}_3\sqrt{|\nu_3|}\right|}, \quad sA_0 = \nu_1 - \nu_3. \tag{B.4}$$

References

Aki, K. and Richards, P. (2002). *Quantitative seismology*, University Science Books.

Boušková, A. (2005). Catalogue of seismic events, Report, Academy of Sciences of the Czech Republic. Online at http://www.ig.cas.cz/seismo/Webnet/.

Červený, V. (2001). *Seismic ray theory*, Cambridge University Press.

Dahm, T., Horálek, J. and Šílený (2000). Comparison of absolute and relative moment tensor solutions for the January 1997 West Bohemia earthquake swarm, *Stud. Geophys. Geod.*, **44**, 233–250.

Fischer, T. (2003). The August-December 2000 earthquake swarm in NW Bohemia: the first results based on automatic processing of seismograms, *J. Geodynamics*, **35**, 59–81.

Fischer, T. and Horálek, J. (2005). Slip-generated patterns of swarm microearthquakes from West Bohemia/Vogtland (Central Europe): Evidence of their triggering mechanism?, *J. Geophys. Res.*, **110**. doi:10.1029/2004JB003363.

Foulger, G. R., Julian, B. R., Hill, D. P., Pitt, A. M., Malin, P. E. and Shalev, E. (2004). Non-double-couple microearthquakes at Long Valley caldera, California, provide evidence for hydraulic fracturing, *J. Volcanol. Geotherm. Res.*, **132**, 45–71. doi:10.1016/S0377-0273(03)00420-7.

Gajewski, D. (1993). Radiation from a point source in general anisotropic media, *Geophys. J. Int.*, **113**, 299–317.

Hainzl, S. and Fischer, T. (2002). Indications for a successively triggered rupture growth underlying the 2000 earthquake swarm in Vogtland/NW Bohemia, *J. Geophys. Res.*, **107**. doi:10.1029/2002JB001865.

Hainzl, S. and Ogata, Y. (2005). Detecting fluid signals in seismicity data through statistical earthquake modeling, *J. Geophys. Res.*, **110**. doi:10.1029/2004JB003247.

Hinzen, K. (2003). Stress field in the Northern Rhine area, Central Europe, from earthquake fault plane solutions, *Tectonophysics*, **377**, 325–356.

Horálek, J., Šílený, J., Fischer, T., Slancová, A. and Boušková, A. (2000). Scenario of the January 1997 West Bohemia earthquake swarm, *Stud. Geophys. Geod.*, **44**, 491–521.

Jost, M. and Herrmann, R. (1989). A student's guide to and review of moment tensors, *Seism. Res. Letters*, **60**, 37–57.

Julian, B., Miller, A. and Foulger, G. (1997). Non-double-couple earthquake mechanisms at the Hengill-Grensdalur volcanic complex, Southwest Iceland, *Geophy. Res. Lett.*, **24**, 743–746.

Kawasaki, I. and Tanimoto, T. (1981). Radiation patterns of body waves due to the seismic dislocation occuring in an anisotropic source medium, *Bull. Seismol. Soc. Am.*, **71**, 37–50.

Klinge, K., Plenefisch, T. and Stammler, K. (2003). The earthquake swarm 2000 in the region Vogtland/NW-Bohemia—earthquake recording at German stations and temporal distribution of events, *J. Geodynamics*, **35**, 83–96.

Málek, J., Horálek, J. and Janský (2005). One-dimensional qP-wave velocity model of the upper crust for the West Bohemia/Vogtland earthquake swarm region, *Stud. Geophys. Geod.*, **49**, 709–730.

Málek, J., Janský, J., Novotný, O., Rößler, D. and the CELEBRATION 2000 working group (2004). Vertically inhomogeneous models of the upper crustal structure in the West-Bohemian seismoactive region inferred from the CELEBRATION 2000 refraction data, *Stud. Geophys. Geod.*, **48**. doi:10.1023/B:SGEG.0000045478.42945.6a.

Menke, W. (1989). *Geophysical data analysis: discrete inverse theory*, Vol. 45 of *International Geophysics Series*, Harcourt Brace Jovanovich.

Novotný, O. (1996). A preliminary seismic model for the region of the West-Bohemian earthquake swarms, *Stud. Geophys. Geod.*, **40**, 353–366.

Parotidis, M., Shapiro, S. and Rothert, E. (2005). Evidence for triggering of the Vogtland swarms 2000 by pore pressure diffusion, *J. Geophys. Res.*, **110**. doi:10.1029/2004JB003267.

Plenefisch, T. and Klinge, K. (2003). Temporal variations of focal mechanisms in the Nový Kostel focal zone (Vogtland/NW-Bohemia)–comparison of the swarms 1994, 1997 and 2000, *J. Geodynamics*, **35**, 145–156.

Pšenčík, I. (1998). ANRAY package, version 4.10, Report, Dept. of Geophysics, Charles University, Prague. Online at http://sw3d.mff.cuni.cz.

Pšenčík, I. and Gajewski, D. (1998). Polarization, phase velocity, and NMO velocity of qP-waves in arbitrary weakly anisotropic media, *Geophysics*, **63**, 1754–1766.

Pšenčík, I. and Teles, T. (1996). Point source radiation in inhomogeneous anisotropic structures, *PAGEOPH*, **148**, 591–623.

Ramos-Martínez, J. and McMechan, G. A. (2001). Source-parameter estimation by full waveform inversion in 3D heterogeneous, viscoelastic, anisotropic media, *Bull. Seismol. Soc. Am.*, **91**, 276–291.

Rößler, D., Krüger, F. and Rümpker, G. (2006). Inversion for seismic moment tensors in anisotropic media using standard techniques for isotropic media, *Geophys. J. Int.*. Submitted.

Rößler, D., Pšenčík, I., Krüger, F. and Rümpker, G. (2005). Retrieval of source parameters for local earthquakes in anisotropic media, Report 15, pp. 333-344, Dept. of Geophysics, Charles University, Prague. Online at http://sw3d.mff.cuni.cz.

Rößler, D., Rümpker, G. and Krüger, F. (2004). Ambiguous moment tensors and radiation patterns in anisotropic media with applications to the modeling of earthquake mechanisms in W-Bohemia, *Stud. Geophys. Geod.*, **48**, 233–250. doi:10.1023/B:SGEG.0000015594.11070.21.

Růžek, B., Vavryčuk, V., Hrubcová, Zedník and the CELEBRATION Working Group (2003). Crustal anisotropy in the Bohemian Massif, Czech Republic: observations based on Central European lithospheric experiment based on refraction (CELEBRATION) 2000, *J. Geophys. Res.*, **108**. doi:10.1029/2002JB002242.

Silver, G. P. and Jordan, T. H. (1982). Optimal estimation of the scalar seismic moment, *Geophys. J. R. astr. Soc.*, **70**, 755–787.

Snoke, J. (2003). FOCMEC: FOcal MEChanism determinations, in *International Handbook of Earthquake and Engineering Seismology*, published by W. Lee, H. Kanamori, P. Jennings and C. Kisslinger, Academic Press, chapter 85.12.

Solomon, S. C. and Julian, B. R. (1974). Seismic constraints on ocean-ridge mantle structure: anomalous fault plane solutions from first motions, *Geophys. J. R. astr. Soc.*, **38**, 265–285.

Sykes, L. R. (1967). Mechanism of earthquakes and nature of faulting on the mid-ocean ridges, *J. Geophys. Res.*, **72**, 5–27.

Vavryčuk, V. (1993). Crustal anisotropy from local observations of shear-wave splitting in West Bohemia, Czech Republic, *Bull. Seismol. Soc. Am.*, **83**, 1420–1441.

Vavryčuk, V. (2001). Inversion for parameters of tensile earthquakes, *J. Geophys. Res.*, **106**, 16339–16355.

Vavryčuk, V. (2002). Non-double-couple earthquakes of 1997 January in West Bohemia, Czech Republic: evidence of tensile faulting, *Geophys. J. Int.*, **149**, 364–373.

Vavryčuk, V. (2005). Focal mechanisms in anisotropic media, *Geophys. J. Int.*, **161**. doi:10.1111/j.1365-246X.2005.02585.

Wirth, W., Plenefisch, T., Klinge, K., Stammler, K. and Seidl, D. (2000). Focal mechanisms and stress field in the region Vogtland/Western Bohemia, *Stud. Geophys. Geod.*, **44**, 126–141.

Tables

Table 1: Coordinates of stations used for source retrieval (see Figure 1).

station	lat. [° North]	lon. [° East]	height [m]	s.r. [Hz]	sensor	institution
KOC	50.26521	12.23352	575	250	SM-3	WEBNET
KRC	50.33159	12.53028	760	250	SM-3	WEBNET
LAC	50.05075	12.62495	838	250	SM-3	WEBNET
LBC	50.26555	12.41218	638	250	SM-3	WEBNET
MANZ	49.98710	12.10950	553	250	STS2	U. Munich
NKC	50.23312	12.44786	564	250	SM-3	WEBNET
P01G	50.240	12.253	750	250	LE-3D/5s	U. Potsdam
P02G	50.319	12.396	630	250	LE-3D/5s	U. Potsdam
P03G	50.270	12.331	800	250	LE-3D/5s	U. Potsdam
P08G	50.225	12.298	710	250	LE-3D/5s	U. Potsdam
P09G	50.188	12.300	720	250	LE-3D/5s	U. Potsdam
P13G	50.411	12.472	480	250	LE-3D/5s	U. Potsdam
SKC	50.16980	12.36103	455	250	LE-3D	WEBNET
SNE	50.31072	12.50273	702	250	SM-3	WEBNET
STC	50.25914	12.51965	666	250	SM-3	WEBNET
TRC	50.30321	12.14452	566	250	LE-3D	WEBNET
VAC	50.23540	12.37710	535	250	SM-3	WEBNET
WERN	50.2874	12.3761	630	250	STS2	U. Leipzig

s.r.=sampling rate, U.=University of, lat./lon.=geographic coordinates

Table 2: Model I. P- (v_p) and S-wave (v_s) velocity as functions of depth (*Málek et al.*, 2005). Cubic-spline interpolation is used. v_s at 32.00 km depth is determined from v_p assuming $v_p/v_s = \sqrt{3}$, density: $\rho = 2650\,\mathrm{kgm}^{-3}$.

depth [km]	0.00	0.41	2.46	8.41	32.00
v_p [kms^{-1}]	3.70	5.37	5.81	6.10	7.20
v_s [kms^{-1}]	2.18	3.16	3.57	3.58	4.16

Table 3: Model II: weak anisotropy (WA) parameters (see *Pšenčík* and *Gajewski*, 1998) used to specify the model (*Málek et al.*, 2005). The WA parameters and reference P-wave velocities taken from model I are used to determine depth distribution of P-wave related parameters. Remaining parameters are determined from S-wave velocities of model I.

WA par.	ϵ_x	ϵ_y	ϵ_z	δ_x	δ_y	δ_z	χ_x	χ_y	χ_z	ϵ_{15}	ϵ_{16}	ϵ_{24}	ϵ_{26}	ϵ_{34}	ϵ_{35}
$\times 10^{-3}$	-12	7	11	-4	6	-5	9	-4	1	2	7	3	7	-7	-5

Table 4: Model III. Density normalised elastic parameters A_{ij} in Voigt notation ($A_{ij} = C_{ij}/\rho$) that describe a homogeneous anisotropic model for West Bohemia.

	A_{11}	A_{12}	A_{13}	A_{22}	A_{23}	A_{33}	A_{44}	A_{55}	A_{66}
$\times 10^6\,\mathrm{m^2s^{-2}}$	23.5	7.8	7.8	31.9	9.9	31.9	11.0	10.8	10.8

Table 5: Residual, slip inclination δ, orientation of the rupture plane, seismic moment M_T ($\mathrm{M}_T = \mathrm{M} * 10^{14}\,\mathrm{Nm}$), and moment-tensor components retrieved by using initial conditions and velocity models I-III. $^{(\star)}$ – inversion without station LBC. Mean slip inclinations $\overline{\delta}$ and standard deviations $\sigma(\delta)$ obtained from bootstrap tests are also given.

		slip inclination [°]			rupture plane [°]				moment tensor [%]		
model	res.	δ	$\overline{\delta}$	$\sigma(\delta)$	strike	dip	rake	M	DC	ISO	CLVD
I	0.06	86.5	86.7	1.2	166	76	-39	3.4	81.0	+4.9	+14.1
I $^{(\star)}$	0.06	87.6	87.8	1.1	168	75	-42	3.5	90.0	+7.8	+2.2
II	0.06	86.8	86.9	1.2	166	76	-40	3.6	82.0	+4.9	+13.1
II$^{(\star)}$	0.06	88.0	87.2	1.2	168	75	-42	3.8	91.5	+8.2	-0.4
III	0.08	83.9	84.1	1.1	168	73	-51	3.2	71.5	+12.7	+15.8
III$^{(\star)}$	0.08	84.3	84.4	1.3	169	73	-52	3.3	74.8	+17.1	+8.2

Figures

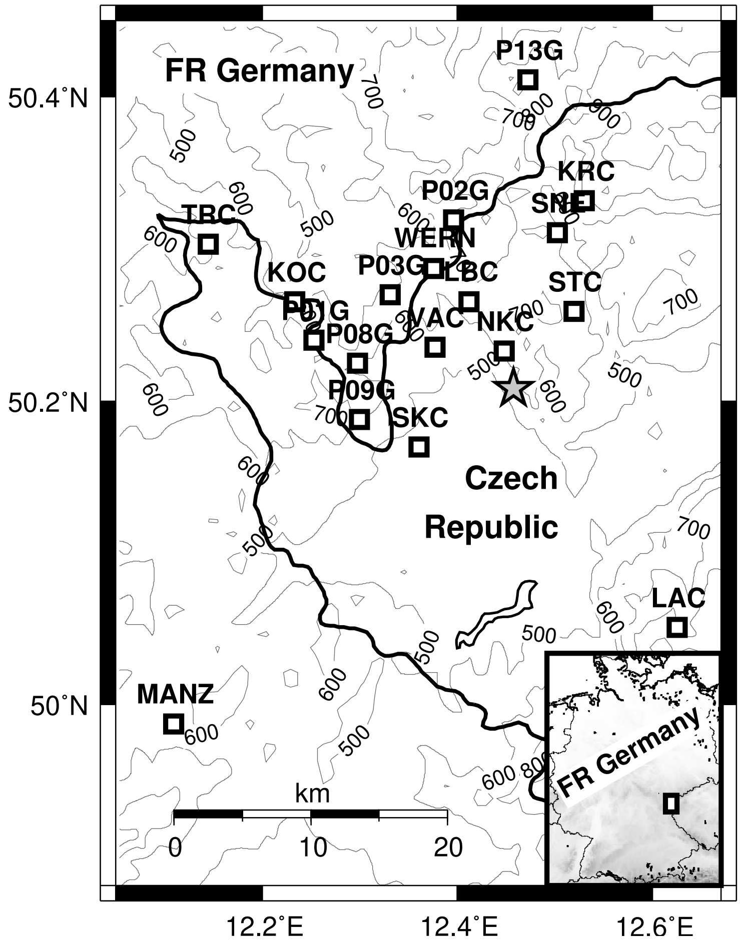

Figure 1: Map of West Bohemia. Star: epicentre at 50.2085°N, 12.4576°E, 9.243 km depth, source time: October 15, 2000, 16:36:48. Squares: stations used for inversion of waveforms.

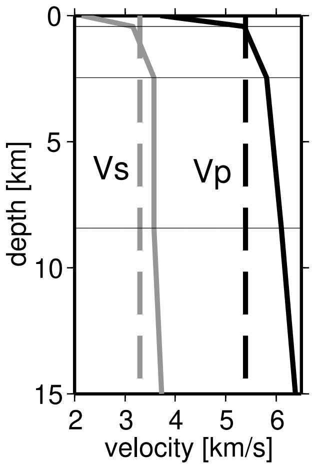

Figure 2: P-wave (black) and S-wave (grey) velocities for West Bohemia (compare Tab. 2). Solid line: vertically inhomogeneous model I (reference velocities for model II) derived by *Málek et al.* (2005). Dashed line: homogeneous transversely isotropic model III characterised by $v_p = \sqrt{(A_{11} + A_{22} + A_{33})/3}$, $v_s = \sqrt{(A_{44} + A_{55} + A_{66})/3}$ (*Vavryčuk*, 1993).

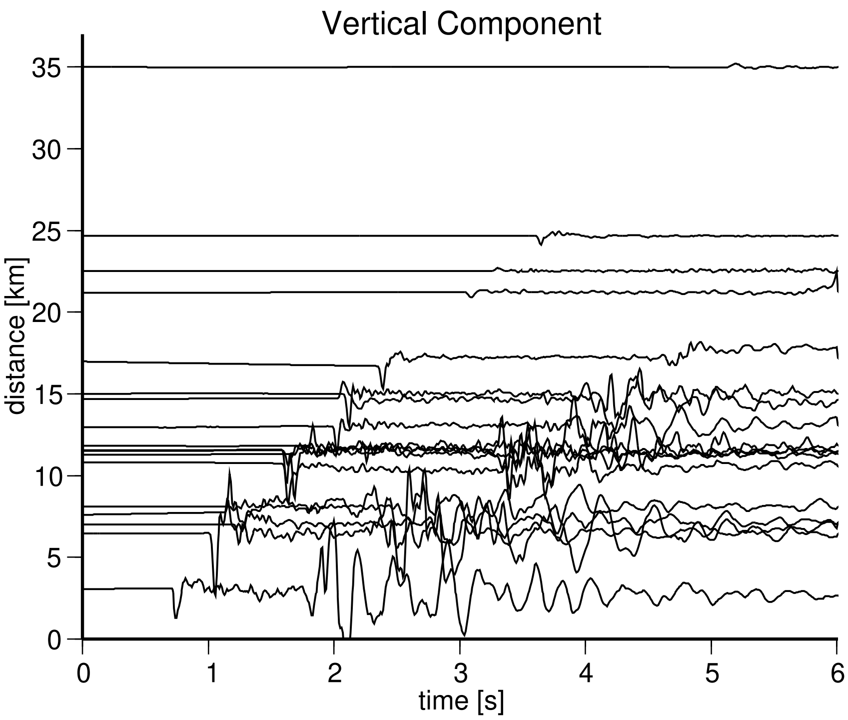

Figure 3: Vertical-component seismograms (displacement) at stations and for event in Fig. 1. Seismograms are unfiltered and sorted by epicentral distance. Positive amplitudes refer to upwards directed displacement. Source time corresponds to -1 s in the seismograms.

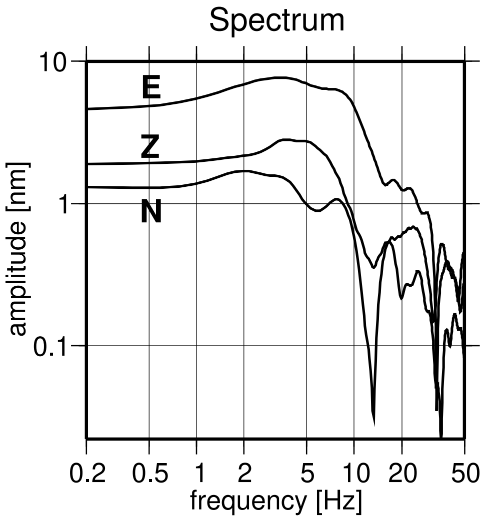

Figure 4: Three-component displacement spectra of the P wave at NKC, the station closest to the epicentre.

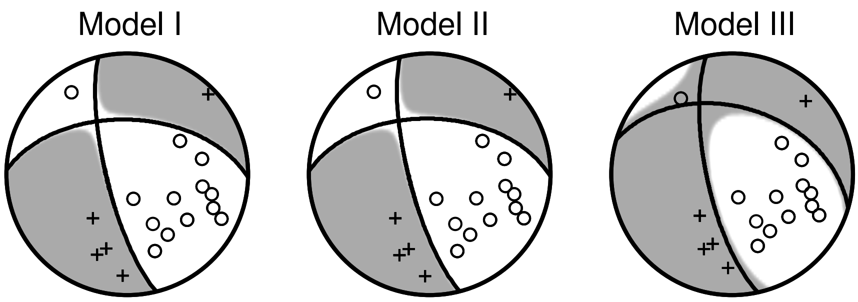

Figure 5: Fault-plane solutions and P-wave radiation patterns for models I, II, and III. Take-off directions of the P waves (lower-hemisphere projection) from the source (star) to the stations (squares) in Fig. 1. First motion of the P waves is compression (grey area, crosses) or dilatation (white area, circles).

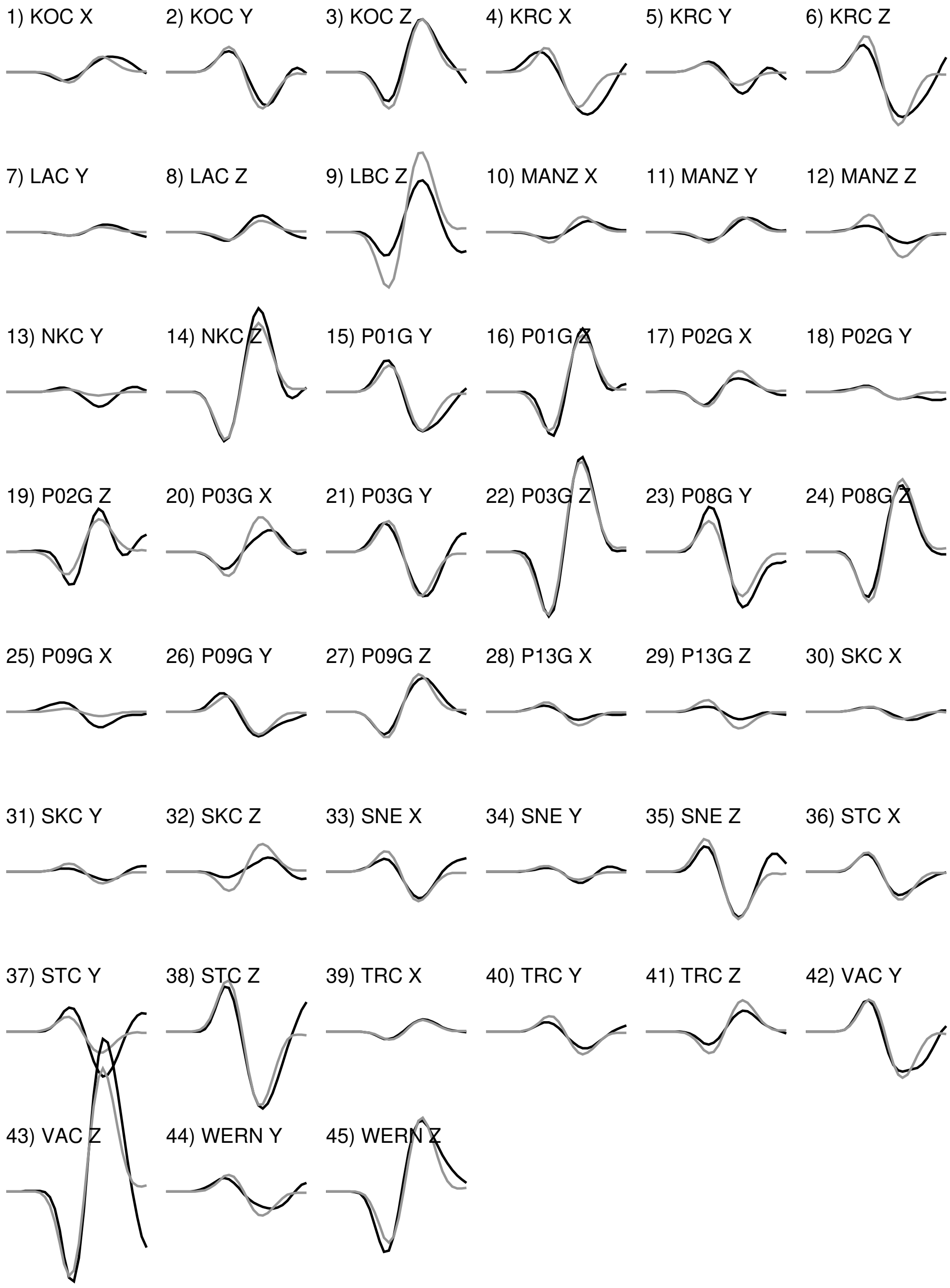

Figure 6: Observed data (black) used during inversion vs. modelled synthetic seismograms (grey) for stations in Fig. 1, 1-10 Hz band-pass filtered. Length of seismograms: 0.4 s, maximum amplitude: 6516 nm at VAC (trace 43). Trace number, station name and component are given above the seismograms. Notation of components: X-North, Y-East, Z-vertical, positive upwards. Note that some components are excluded from inversion due to low correlation between data and synthetics.

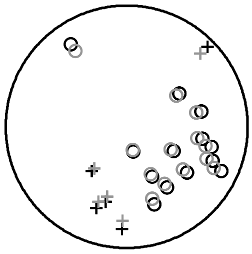

Figure 7: Comparison of take-off directions of the P waves in Fig. 5 (lower-hemisphere projection) for the models II (black), and III (grey). Take-off directions for P waves in model I from Fig. 5 are not plotted. They are indistinguishable from take-off directions in model II. First motion is compression (crosses) or dilatation (circles).

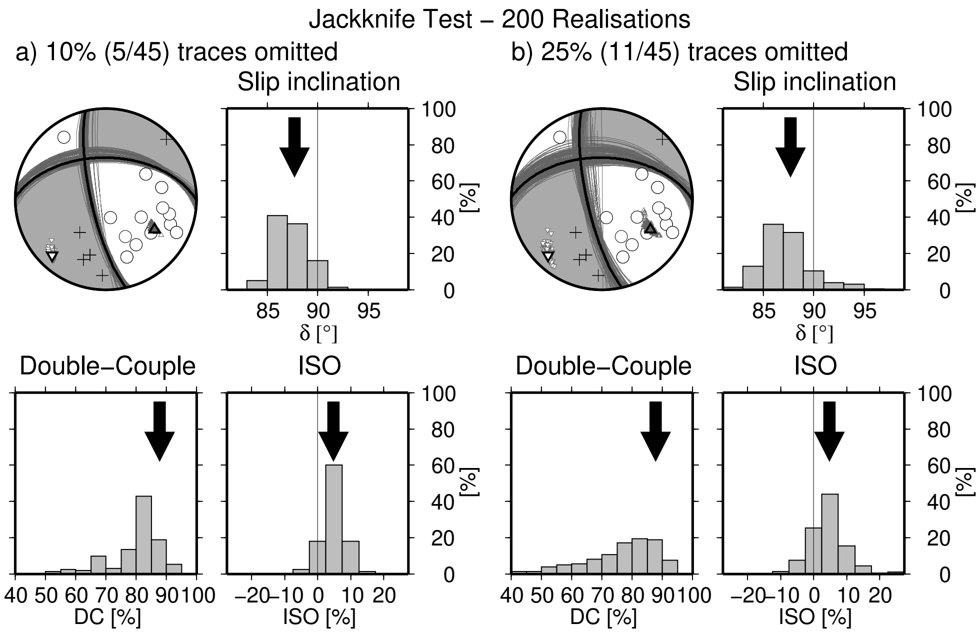

Figure 8: Jackknife tests for event (star) and stations (squares) in Fig. 1 using model II. In 200 realisations, a) 10% (left) and b) 25% (right) of all available traces are randomly omitted for inversion. Fault-plane solutions with P and T axes (grey triangles and grey inverted triangles, respectively) are plotted for each realisation (grey lines) as well as the distribution of corresponding slip inclinations (δ) and moment-tensor components (DC, ISO). For unmodified conditions,fault-plane solutions and the P and T axes are plotted in black, the radiation pattern due to the retrieved source is underlying the fault-plane solutions (grey area: compression, white area: dilatation), and corresponding quantities are indicated by arrows.

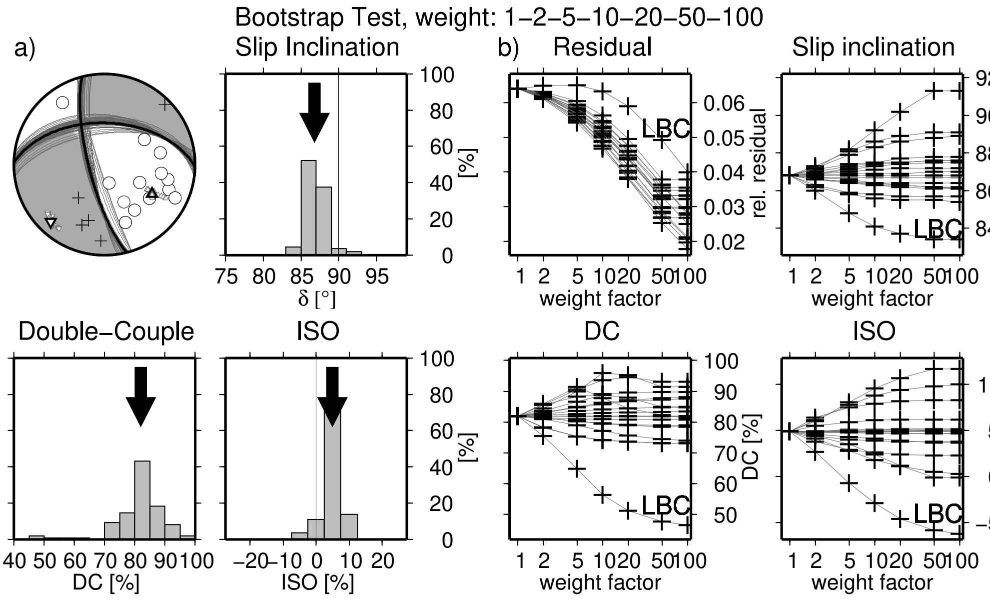

Figure 9: Bootstrap tests for event (star) and stations (squares) in Fig. 1 using model II. During every realisation the weight of each station is varied (weight factors: 1, 2, 5, 10, 20, 50, 100) while the weight of remaining stations is one. The procedure is repeated for each station. a) Fault-plane solutions and source parameters retrieved by bootstrapping. See Fig. 8 for more details. b) Results for bootstrapping of individual stations (one curve - one station). Along every curve the weight of another station is varied while the weight of the remaining stations is kept constant, equal one. Note outliers for bootstrapping of station LBC.

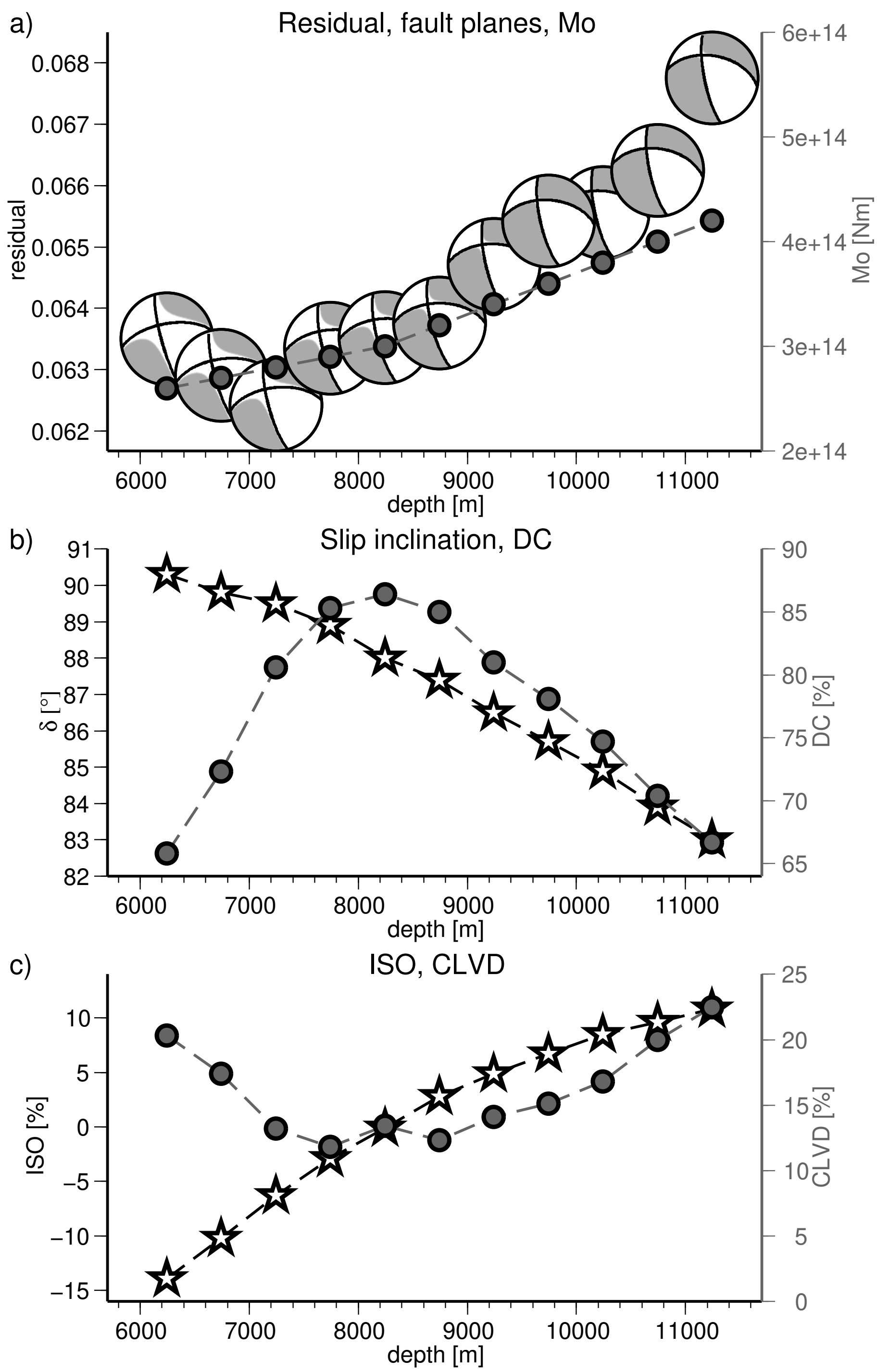

Figure 10: Source parameters as a function of varying depth obtained from inversions assuming model I, epicentre position and stations in Fig. 1 but different source depths. Localised source depth: 9.243 km. a) Fault-plane solutions positioned at residual values R and seismic moments M_T (circles). b) Slip inclinations δ (stars) and double-couple moment-tensor components DC (circles). c) Isotropic moment-tensor components ISO (stars) and compensated linear vector dipole components CLVD (circles).

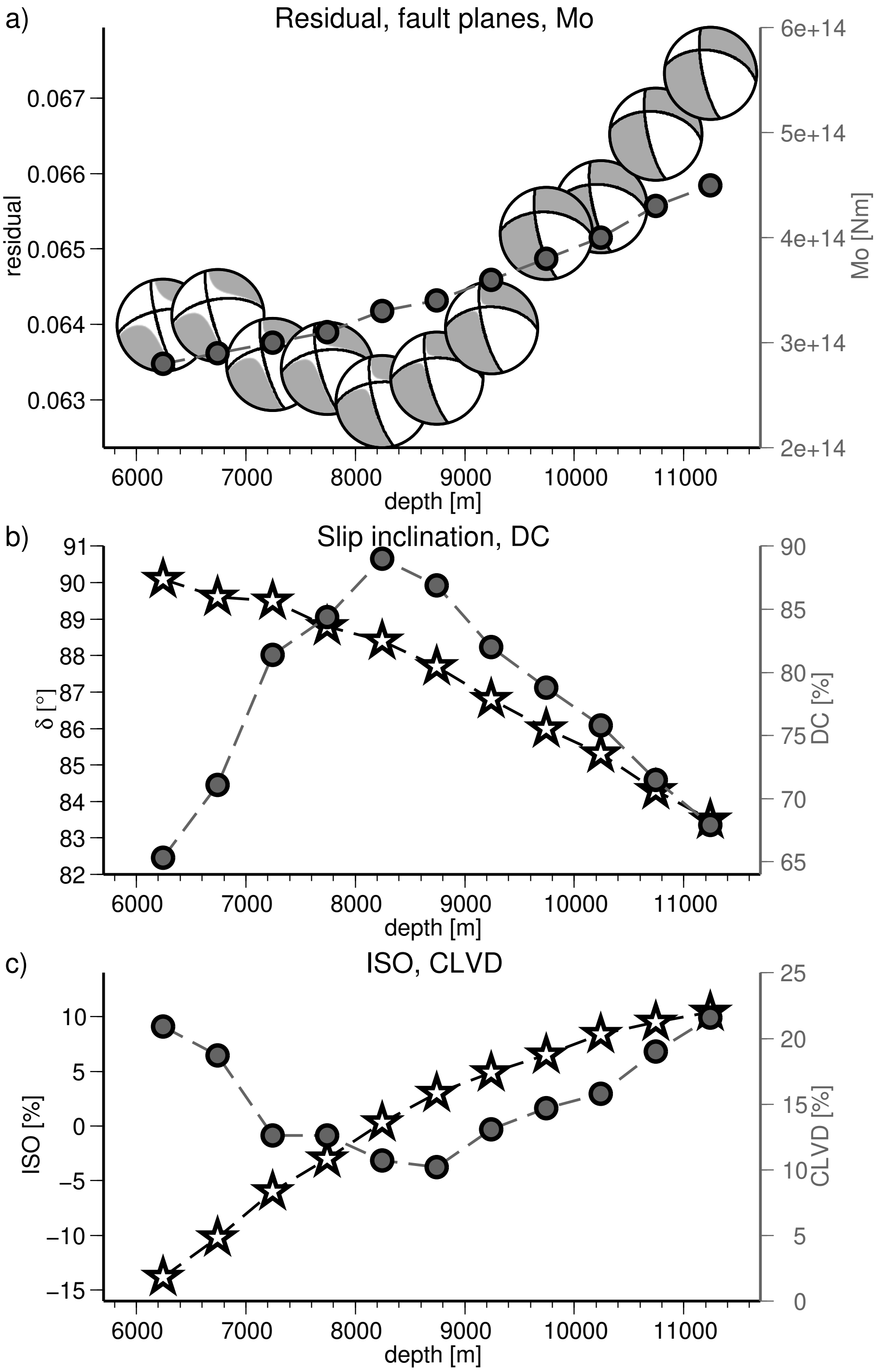

Figure 11: As in Fig. 10 but for model II.

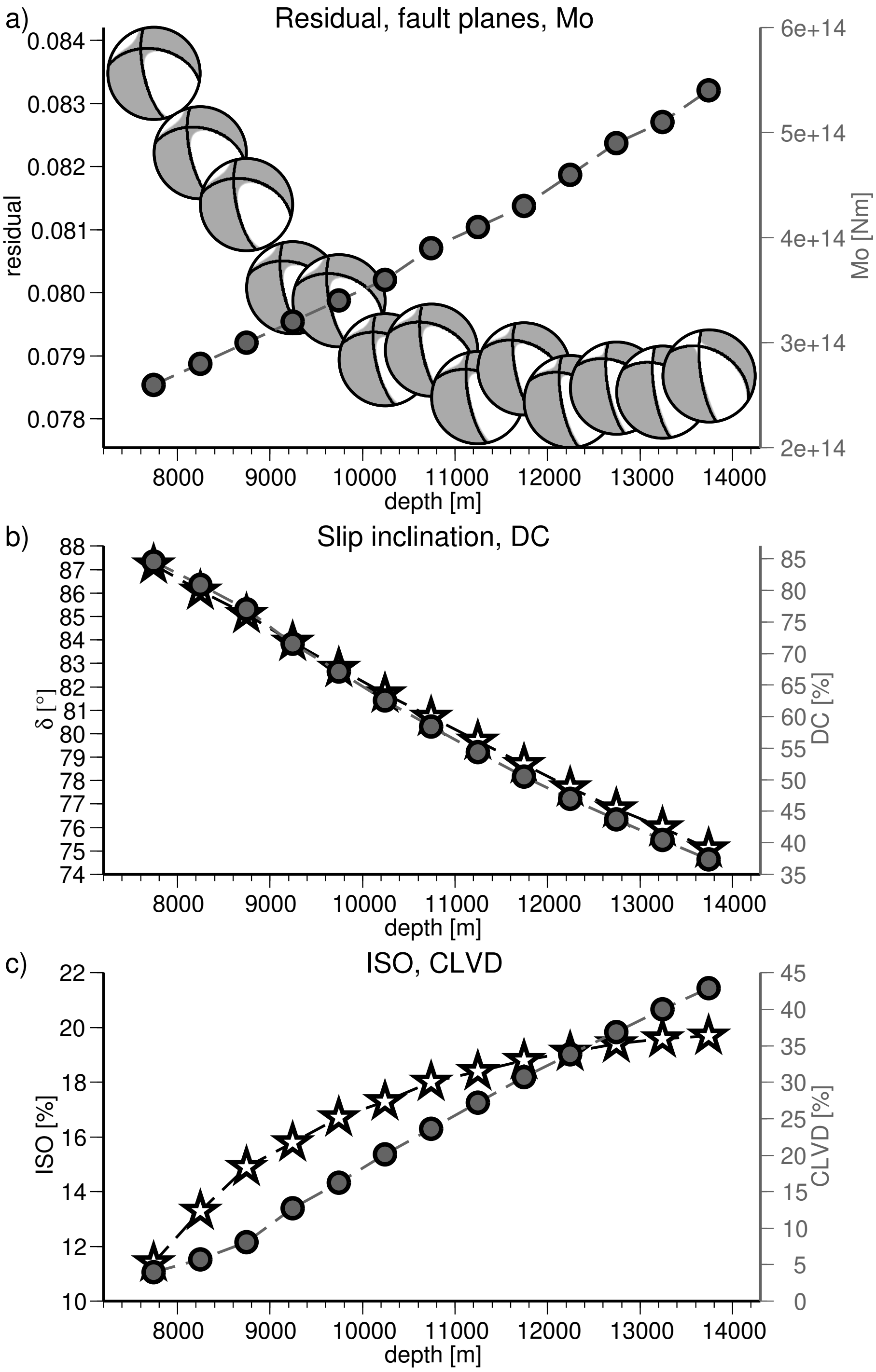

Figure 12: As in Fig. 10 but for model III.